A new fission mode in ^{220}Ra

Misty K. Lakelin[1,*], Kaitlin J. Cook[1], Jacob Buete[1], David J. Hinde[1], Mahananda Dasgupta[1], Lauren T. Bezzina[1,**], Sophie L. Hayles[1], Hyeonseop Lee[1], Caroline C. Seabra[1], Tony Tran[1], and Maggie M. Webber[1]

[1]Department of Nuclear Physics and Accelerator Applications, The Australian National University, Canberra, ACT 2601, Australia

Abstract. Shell-driven fission modes result from the quantum mechanical many-body dynamics underlying nuclear fission. Their regions of influence, as well as the nuclear shapes they induce at scission, is a rapidly developing area of research. Evidence has emerged of novel fission modes in pre-actinide nuclei associated with $Z\approx36$ and $Z\approx44$. We present evidence of the Z=44 mode persisting up to ^{220}Ra (Z=88). Being an example of bimodal symmetric fission, this result necessitated two-dimensional Gaussian fitting and a statistically rigorous data subsampling analysis to separate this novel mode from the liquid drop mode.

1 Introduction

When a nucleus undergoes fission it elongates and splits into two separate fragment nuclei. Interplay between macroscopic forces (Coulomb repulsion and the strong nuclear force) and microscopic quantum shell effects dictate the nucleus' evolution towards scission and thus its final configuration. However, thermal fluctuations within this system lead to broad distributions of possible scission configurations. Experimentally, nuclear shapes at scission are primarily understood through two key observables: fragment mass-ratio ($M_R = \frac{m_1}{m_1+m_2}$) which quantifies the splitting of mass between fragments, and fragment total kinetic energy (TKE) which characterises the elongation of the scission configuration via Coulomb repulsion. Certain scission configurations are more energetically favourable than others and manifest as Gaussian-like distributions of M_R and TKE. These are known as fission modes [1].

Actinide nuclei are known to exhibit three fission modes [1]. The first is the liquid drop mode (LDM), which results from macroscopic forces and produces symmetric mass splits and an elongated scission configuration. The other two are shell-driven modes — resulting from the addition of microscopic shell effects — associated with octupole-deformed proton shells $Z\approx52$ and $Z\approx56$ [2, 3], referred to as Standard I (StI) and Standard II (StII), respectively.

Evidence has been mounting of new fission modes driving asymmetric fission in sub-lead and sub-actinide nuclei since 2010, when asymmetric fission was first observed in ^{180}Hg [4]. Studies of single nuclei [5, 6] and isotopic chains [7–9] have observed these new modes and attributed them to quadrupole deformed proton shells around Z=36 and Z=44 [10]. A recent, large-scale study has observed the Z=36 mode as low as ^{144}Gd and persisting thereafter, with the Z=44 mode emerging and taking dominance around Hg and persisting until Th [11]. Another study has mapped an island of Z=36-driven asymmetric fission around Hg and Tl [12]. These works demonstrate the rapidly expanding interest in these novel modes.

In their study of ^{178}Pt fission, Swinton-Bland et al. [5] demonstrated the effectiveness of two-dimensional Gaussian fitting to fragment mass and a linearised measure of TKE — relative total kinetic energy (RTKE) — in finding evidence of fission modes. This allows the relative nuclear elongation at scission to be compared between modes without requiring absolute TKE measurements.

In the present study, we make use of this technique to search for the $Z\approx44$ mode in ^{220}Ra (Z=88). The atomic number of Ra is 2×44 so this would be an instance of bimodal symmetric fission; both the LDM and the $Z\approx44$ mode are expected to overlap entirely in distributions of M_R. Since the $Z\approx44$ mode fragments are expected to be quadrupole deformed [10], the mode's scission configuration may be more compact than the LDM and hence distinct from it in distributions of RTKE, as this paper will demonstrate.

2 Experiment

The 14UD Pelletron accelerator at the Heavy Ion Accelerator Facility at the Australian National University supplied ^{12}C beams with energies between 60 and 80 MeV. This energy range was divided into 2 MeV steps to observe the persistence and evolution with excitation energy of any modes present. With the beam bombarding a ^{208}PbS target (areal density 184 μg/cm^2), ^{12}C and ^{208}Pb fuse to form ^{220}Ra with excitation energies above the ground-state between 24.5 and 43.5 MeV.

The CUBE spectrometer was used to detect the fission fragments of ^{220}Ra in coincidence. Three position sensitive multi-wire proportional counters (MWPCs) of CUBE were used and configured as in Ref. [13]: two

*e-mail: Misty.Lakelin@anu.edu.au
**Present address: Laboratory of Ion Beam Physics, ETH Zürich, HPK G 31, Otto-Stern-Weg 5, 8093 Zürich, Switzerland

279.0 mm × 357.0 mm MWPCs centred at 45° and 90° relative to the beam axis, and one 131.5 mm × 357.0 mm MWPC at 135°. The resulting π solid angle coverage, as well as the choice of reaction, enabled at least one million fission events to be recorded per energy step.

Calibration and a kinematic reconstruction produced the fragment velocity vectors in the centre-of-mass frame at scission which are related to the fragment mass ratio by

$$M_R = \frac{m_2}{m_1 + m_2} = \frac{v_{1,cm}}{v_{1,cm} + v_{2,cm}}, \quad (1)$$

and to the fragment total kinetic energy by

$$\mathrm{TKE} = \frac{1}{2} m_1 v_{1,cm}^2 + \frac{1}{2} m_2 v_{2,cm}^2. \quad (2)$$

This process, which relies on precise (~0.1 ns) timing calibration adjustments, leads to slight shifts in TKE and cannot yet yield extremely accurate absolute TKE measurements. Instead, we compare changes in a measure of relative TKE across single measurements.

3 Results

3.1 RTKE and empirical evidence for shell-driven symmetric fission

TKE is expected to have a parabolic dependence on Z and A via the Coulomb force. Viola systematics [14] are a fit based on the compound nucleus proton and nucleon number Z_{CN}, A_{CN} to a large body of TKE measurements from across the nuclear chart. The following equation is an extension of these systematics to the nascent fragments with proton and nucleon numbers $Z_{1,2}$, $A_{1,2}$ and is an empirical description of the most probable kinetic energy release from fission [15]:

$$\mathrm{TKE_{Viola}} = 0.755 \frac{Z_1 Z_2}{A_1^{1/3} + A_2^{1/3}} + 7.3\ \mathrm{MeV}. \quad (3)$$

Figure 1(a) shows the M_R-TKE distribution for measured ^{220}Ra fission events at excitation energy $E^* = 24.5$ MeV. The solid black line shows $\mathrm{TKE_{Viola}}$ for this system. Taking the ratio of measured TKE values to $\mathrm{TKE_{Viola}}$ and parametrising in terms of M_R via the unchanged charge distribution assumption [16] (N/Z of the compound nucleus is maintained for the fragments) yields the RTKE:

$$\mathrm{RTKE}(M_R) = \frac{\mathrm{TKE_{measured}}(M_R)}{\mathrm{TKE_{Viola}}(M_R)}. \quad (4)$$

The distribution of M_R and RTKE for the same events is shown in Figure 1(b). RTKE is a more effective proxy of nuclear shape than TKE as it removes the parabolic dependence on M_R and allows direct comparisons of scission elongation within a dataset. It is easier to see the high RTKE contributions near M_R<0.4 and M_R>0.6 in this distribution by its curved shape. This is further emphasised in Figure 1(c) where we show the mean RTKE against M_R. Pokrovsky et al. [17] observed high TKE contributions in this region in their measurements of ^{220}Ra fission and used

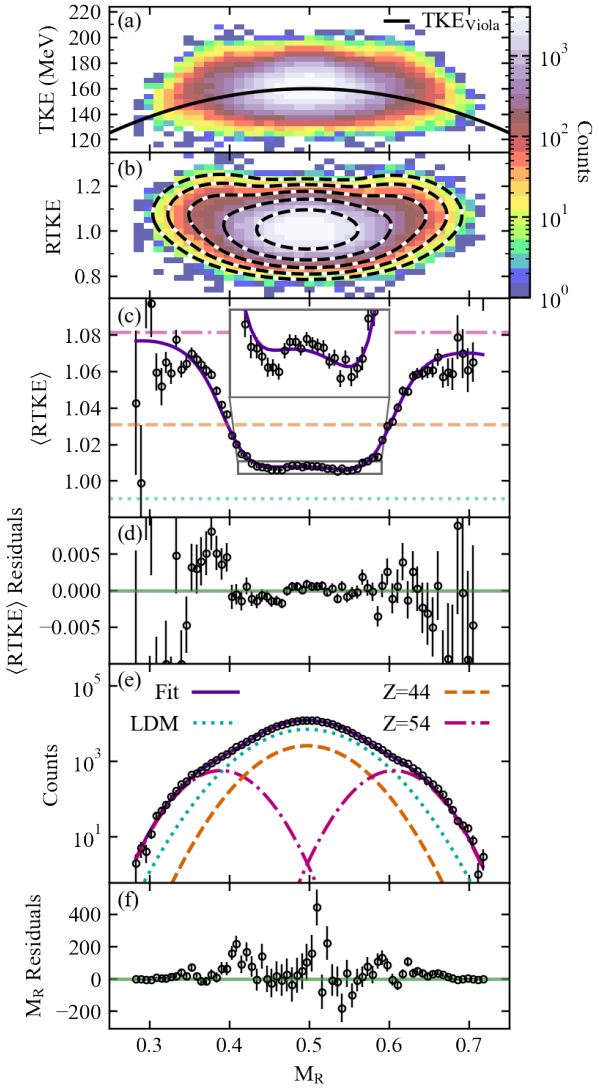

Figure 1. Experimental results and a best fit to the ^{220}Ra fission events at E^*=24.5 MeV. (a) The two-dimensional M_R-TKE distribution with $\mathrm{TKE_{Viola}}$, the expectation from systematics [14], shown in solid black. These are not absolute TKE measurements since they incur a shift from the calibration method (see the text for details). (b) The two-dimensional M_R-RTKE distribution with the contours of the fit shown by black and white dashed lines. (c) The mean RTKE vs. M_R. The complete fit to the data is shown by solid purple with contributions from the LDM (dotted blue), and an inner (dashed orange) and outer (dash-dotted pink) shell driven mode. The contributions of each fitted mode manifest as horizontal lines corresponding to their RTKE centroids. The inset axes show 0.4<M_R<0.6 and 1.004<⟨RTKE⟩<1.011. The tilt in ⟨RTKE⟩ with M_R is discussed in the text. (d) The residuals of the fit to the above distribution. (e) The projection of panel (b) in M_R. (f) The residuals of the fit to the above distribution.

a slicing and Gaussian fitting method to attribute them to the StI and StII modes.

The inset axes within Figure 1(c) show an expanded vertical scale for 0.4<M_R<0.6. The mean RTKE values around M_R=0.5 are higher than those at M_R=0.45 and M_R=0.55; this is not within the error of the data or its scat-

ter. This structure is also present and statistically significant in distributions of mean RTKE for data recorded at each E^*. A given fission mode has only one mean RTKE value for all M_R values, so for this structure to exist in distributions of mean RTKE implies there are two modes around symmetry contributing a high RTKE component and a low RTKE component. If the LDM is contributing the low RTKE component, then the *high* RTKE component comes from a shell-driven mode centred at mass-symmetry with a more *compact* shape than the LDM. Alternatively, if the LDM is contributing the high RTKE component, then the *low* RTKE component comes from a shell-driven mode centred slightly offset from mass-symmetry with a more *elongated* shape than the LDM — which would be extremely elongated. We can determine which of these two possibilities is most likely to be correct with two-dimensional M_R-RTKE fitting.

3.2 Two-dimensional Gaussian fitting

A two-dimensional Gaussian fit to all ^{220}Ra fission events at E^*=24.5 MeV is shown in Figure 1(b) in black and white contours, and projected onto M_R in Figure 1(e). Following techniques used in Ref. [5], we determined the best fit to be composed of an assumed LDM whose M_R centroid was fixed to the symmetry plane of the data, and two unfixed (asymmetric) modes that were allowed to vary in M_R. The outermost of these modes corresponds to a heavy fragment with mean Z=53.4 and RTKE=1.08 (comparatively, the mean RTKE of the fitted LDM is 0.99). This corresponds to the high RTKE contributions of both the StI and StII modes which have previously been established in ^{220}Ra [17]. The innermost of these unfixed modes is centered at symmetry (Z=44) with a mean RTKE higher than that of the LDM, and thus has a more compact shape at scission. Due to the strong overlap in the LDM and this compact symmetric mode, there are large uncertainties in the share of yield between each fitted mode. This relative strength is unlikely to be resolved accurately with a single fitting analysis. A fit parameter allowing a small linear dependence of RTKE on M_R was included, to account for minor calibration uncertainties (see Figure. 1(c)).

3.3 Data subsampling

In a study of multichance fission, Berriman et al. [18] demonstrated that Gaussian fitting can introduce significant uncertainties into fine-detail analyses. Therefore, considering the significant overlap expected (and shown in Figure. 1(e)) between the proposed $Z\approx44$ mode and the LDM in ^{220}Ra, we approach the application of Gaussian fitting with caution. To bolster the statistical rigour of the analysis, we employed data subsampling [19]. A high statistics measurement typically only culminates in a single fitting result which forms the basis of a fission mode analysis. Alternatively, performing fits to multiple random subsamples of fission events produces a distribution of different possible results corresponding to different χ^2 minima found by the fitting procedure. This analysis shows a more complete picture of the various structures present in the total data and their possible interpretations via Gaussian fitting. The correct interpretation and hence the true modes present will be the most likely result to appear from the multiple fits.

For each E^*, 10^5 fission events were selected from the total dataset at random, and a three-mode, two-dimensional Gaussian fitting procedure applied (as described in Section 3.2). This process was repeated 200 times for each E^* with replacement of the selected events.

Figure 2(a) and (b) are histograms of the mean heavy fragment Z of the fitted inner and outer fission modes, respectively, resulting from this process. The inner mode Z is strongly peaked at Z=44 for all energies, with a tail tending towards higher Z. This tail is comprised of results from higher energies as seen from the colour scale. The anticipated Z=44 mode is shell-driven, and hence attenuates at higher excitation energies due to shell-damping. This attenuation makes it increasingly difficult for the fitting algorithm to distinguish the Z=44 mode from the LDM, so the fitted inner mode shifts away from symmetry.

An isolated subset of fits placed this inner mode around Z=53 (Figure. 2(a)), a contribution from StI fission. Figure 2(c) shows the correlation between the inner and outer mode Z values. The upper right cluster in this figure demonstrates that these StI fits are paired with fitted outer modes shifted to higher Z, around Z=56 (closer to StII fission). Therefore, this subset of fits is distinguishing both the StI and StII fission modes, with no additional shell-driven mode at symmetry.

As stated in Section 2, different datasets have different calibrations and hence slight offsets in TKE and RTKE. To compare the RTKE centroids of fits from different datasets, we normalised them to their respective LDM RTKE centroids, yielding $RTKE_{norm}$. Therefore, these $RTKE_{norm}$ values show scission elongations compared to the LDM such that $RTKE_{norm}>1$ is more compact than the LDM, and $RTKE_{norm}<1$ is more elongated than the LDM. Figure 2(d) and (e) show distributions of the fitted inner and outer mode Z values with these $RTKE_{norm}$ values. In panel (d), the Z=44 peak generally has $RTKE_{norm}>1$, showing a compact configuration. Only a small subset of fits have Z=44 and $RTKE_{norm}<1$ — the alternative highly elongated configuration. The other small subset with $Z \sim 53$ (Figure. 2(d)) identified with the StI mode also have $RTKE_{norm}>1$ which is expected for standard fission. Similarly, Figure 2(e) shows the $RTKE_{norm}$ of the outer modes tend towards high RTKE and compact shapes in agreement with standard fission.

To evaluate and summarise the findings from these 2000 fits, three fission mode configurations were present:

1. The most common configuration of modes, which makes up 48.9% of the total fits and is persistent at all beam energies, resolved a compact mode exactly at symmetry (Z=44 with $RTKE_{norm}>1$), with a further 33.6% near symmetry between $45\leq Z<50$. Together these fits make up 82.5% of the results. These fits also found a single asymmetric mode reflecting the sum of StI and StII, and the LDM.

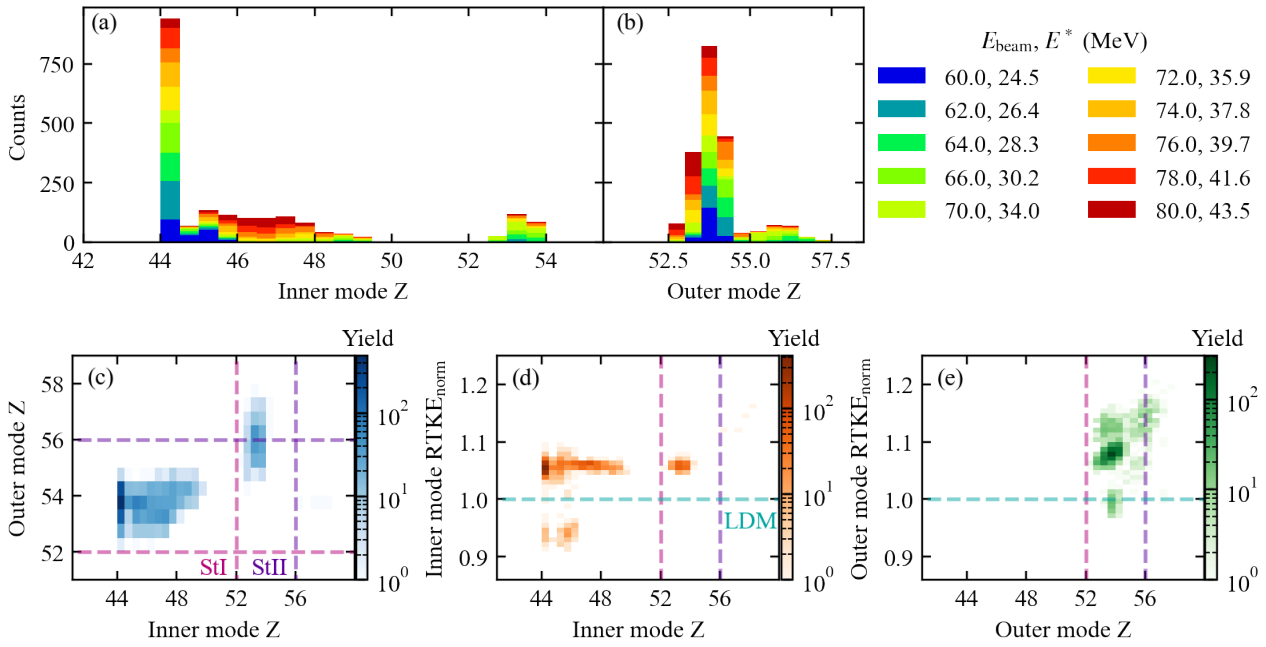

Figure 2. The results of 2000 subsampled two-dimensional Gaussian fits across 10 excitation energies of fissioning ^{220}Ra. These results concern the two unfixed modes of the fit and do not include the fixed LDM (see the text for details). The dataset corresponding to a beam energy of 68 MeV or E^*=32.1 MeV was discounted due to low measurement resolution caused by an isolated experimental error. (a) A histogram of the mean heavy fragment Z of each innermost mode. (b) A histogram of the mean heavy fragment Z of each outermost mode. (c) Two-dimensional distribution of the heavy fragment Z of each innermost mode with that of each outermost mode. Approximate proton numbers associated with StI (52) and StII (56) are shown by dashed pink and purple lines, respectively. (d) Two-dimensional distribution of the heavy fragment Z of each innermost mode with its normalised RTKE centroid (see the text for details). The LDM (RTKE$_{norm}$=1) is shown by a dashed blue line. (e) Two-dimensional distribution of the heavy fragment Z of each outermost mode with its normalised RTKE centroid.

2. 12.0% of fits resolved both StI and StII modes individually (alongside the LDM) with both modes having Z>52 and RTKE$_{norm}$>1.

3. The least common configuration of modes, 1.8%, resolved a highly elongated inner mode with 44≤Z<50 and RTKE$_{norm}$<1 (alongside the LDM and a standard mode). This was the possible alternative to a compact symmetric mode presented from empirical evidence in Section 3.1.

The remaining fits were not physically consistent. As noted in this analysis, the spread across these parameters shows the sensitive competition between Gaussian modes during the fitting process. Fitting does not gravitate Gaussians towards fission modes but rather regions of high yield. This is why some fits in this analysis found a sum of the StI and StII modes as opposed to fitting to either one. Correlations between fitting parameters will become increasingly impactful as fission mode analyses focus on high statistics measurements to find new modes in regions of strong overlap — such as the present study analysing four fission modes of ^{220}Ra. However, the impact of these correlations on fission mode analyses can be reduced by leading with close empirical analyses, and by using statistically rigorous techniques such as data subsampling.

4 Summary and Outlook

In this paper, we discuss evidence of a novel compact symmetric fission mode in ^{220}Ra, likely driven by the quadrupole deformed Z=44 proton shell, and the importance of two-dimensional Gaussian fitting and data subsampling to this result. Empirical evidence of this mode can be seen in distributions of mean RTKE by a distinct narrow raised structure at mass-symmetry that persists across E^*=24.5–43.5 MeV.

This structure could have been attributed to a compact symmetric mode or a highly elongated asymmetric mode. To extract the likelihood of each, we performed a two-dimensional Gaussian fitting and data subsampling analysis. The most common result from 82.5% of the 2000 fits of sampled data resolved a compact symmetric mode, whereas only 1.8% resolved a highly elongated asymmetric mode near symmetry. These statistics indicate the presence of a compact symmetric mode in ^{220}Ra fission. This result joins a mounting set of evidence for a new fission mode driven by this shell in pre-actinide nuclei. It is also among the first pieces of evidence of bimodal symmetric fission below ^{258}Fm [20].

It remains to search for this mode across the Ra isotopic chain which may provide more evidence of its shell

origins. Neighbouring nuclei are being analysed to explore the bounds of this shell's influence, p articularly i n conjunction to the established StI and StII shell-driven modes (see Ref. [11]), though much more data is required to establish this mode as strongly as the standard fission modes.

Acknowledgements

This work was supported by Australian Research Council Grants DP200100601, DE230100197 and DP230101028, DP250101791. The authors acknowledge the facilities, and the scientific a nd t echnical a ssistance p rovided by Heavy Ion Accelerators (HIA). HIA is supported by the Australian Government through the National Collaborative Research Infrastructure Strategy (NCRIS) program. S.L.H., H.L., M.M.W acknowledge support from an Australian Government Research Training Program (RTP) Scholarship.

References

[1] U. Brosa, S. Grossmann, A. Müller, Nuclear scission, Phys. Rep. **197**, 167 (1990). 10.1016/0370-1573(90)90114-H

[2] G. Scamps, C. Simenel, Impact of pear-shaped fission fragments on mass-asymmetric fission in actinides, Nature **564**, 382 (2018). 10.1038/s41586-018-0780-0

[3] C. Böckstiegel, S. Steinhäuser, K.H. Schmidt, H.G. Clerc, A. Grewe et al., Nuclear-fission studies with relativistic secondary beams: Analysis of fission channels, Nucl. Phys. A **802**, 12 (2008). 10.1016/j.nuclphysa.2008.01.012

[4] A.N. Andreyev, J. Elseviers, M. Huyse, P. Van Duppen, S. Antalic et al., New type of asymmetric fission in proton-rich nuclei, Phys. Rev. Lett. **105**, 252502 (2010). 10.1103/PhysRevLett.105.252502

[5] B.M.A. Swinton-Bland, J. Buete, D.J. Hinde, M. Dasgupta, T. Tanaka et al., Multi-modal mass-asymmetric fission of ^{178}Pt from simultaneous mass-kinetic energy fitting, Phys. Lett. B **837**, 137655 (2023). 10.1016/j.physletb.2022.137655

[6] E. Prasad, D.J. Hinde, K. Ramachandran, E. Williams, M. Dasgupta et al., Observation of mass-asymmetric fission of mercury nuclei in heavy ion fusion, Phys. Rev. C **91**, 064605 (2015). 10.1103/PhysRevC.91.064605

[7] B.M.A. Swinton-Bland, M.A. Stoyer, A.C. Berriman, D.J. Hinde, C. Simenel et al., Mass-asymmetric fission of ^{205,207,209}Bi at energies close to the fission barrier using proton bombardment of ^{204,206,208}Pb, Phys. Rev. C **102**, 054611 (2020). 10.1103/PhysRevC.102.054611

[8] E. Prasad, D. Hinde, M. Dasgupta, D. Jeung, A. Berriman et al., Systematics of the mass-asymmetric fission of excited nuclei from 176Os to 206Pb, Phys. Lett. B **811**, 135941 (2020). 10.1016/j.physletb.2020.135941

[9] A.A. Bogachev, E.M. Kozulin, G.N. Knyazheva, I.M. Itkis, M.G. Itkis et al., Asymmetric and symmetric fission of excited nuclei of ^{180,190}Hg and ^{184,192,202}Pb formed in the reactions with ^{36}Ar and ^{40,48}Ca ions, Phys. Rev. C **104**, 024623 (2021). 10.1103/PhysRevC.104.024623

[10] G. Scamps, C. Simenel, Effect of shell structure on the fission of sub-lead nuclei, Phys. Rev. C **100**, 041602 (2019). 10.1103/PhysRevC.100.041602

[11] J. Buete, B.M.A. Swinton-Bland, D.J. Hinde, K.J. Cook, M. Dasgupta et al., Universality of shell effects in fusion-fission mass distributions, Phys. Lett. B **865**, 139459 (2025). 10.1016/j.physletb.2025.139459

[12] P. Morfouace, J. Taieb, A. Chatillon, L. Audouin, G. Blanchon et al., An asymmetric fission island driven by shell effects in light fragments, Nature **641**, 339 (2025). 10.1038/s41586-025-08882-7

[13] T. Banerjee, D.J. Hinde, D.Y. Jeung, K. Banerjee, M. Dasgupta et al., Systematic evidence for quasi-fission in ^{9}Be–, ^{12}C–, and ^{16}O-induced reactions forming ^{258,260}No, Phys. Rev. C **102**, 024603 (2020). 10.1103/PhysRevC.102.024603

[14] V.E. Viola, K. Kwiatkowski, M. Walker, Systematics of fission fragment total kinetic energy release, Phys. Rev. C **31**, 1550 (1985). 10.1103/PhysRevC.31.1550

[15] D.J. Hinde, J.R. Leigh, J.J.M. Bokhorst, J.O. Newton, R.L. Walsh et al., Mass-split dependence of the pre- and post-scission neutron multiplicities for fission of ^{251}Es, Nucl. Phys. A **472**, 318 (1987). 10.1016/0375-9474(87)90213-2

[16] A.C. Wahl, R.L. Ferguson, D.R. Nethaway, D.E. Troutner, K. Wolfsberg, Nuclear-charge distribution in low-energy fission, Phys. Rev. **126**, 1112 (1962). 10.1103/PhysRev.126.1112

[17] I.V. Pokrovsky, L. Calabretta, M.G. Itkis, N.A. Kondratiev, E.M. Kozulin et al., Three fission modes of ^{220}Ra, Phys. Rev. C **60**, 041304 (1999). 10.1103/PhysRevC.60.041304

[18] A.C. Berriman, D.J. Hinde, D.Y. Jeung, M. Dasgupta, H. Haba et al., Energy dependence of p +^{232} Th fission mass distributions: Mass-asymmetric standard I and standard II modes, and multi-chance fission, Phys. Rev. C **105**, 064614 (2022). 10.1103/PhysRevC.105.064614

[19] B. Efron, Bootstrap methods: Another look at the jackknife, Ann. Stat. **7**, 1 (1979). 10.1214/aos/1176344552

[20] E.K. Hulet, J.F. Wild, R.J. Dougan, R.W. Lougheed, J.H. Landrum et al., Bimodal symmetric fission observed in the heaviest elements, J. Less-Common Met. **122**, 469 (1986). 10.1016/0022-5088(86)90443-1